

## FIBRE OPTIC CODED DETECTOR SYSTEMS ON THE SNS

P L Davidson, N Rhodes and H Wroe

### 1. INTRODUCTION

The principle of the fibre optic coded scintillator detector has been described elsewhere<sup>[1],[2]</sup>. Systems using this principle have been built for two SNS instruments, the High Resolution Powder Diffractometer (HRPD) and the Low Q Spectrometer (LOQ). This paper gives brief details of these detector systems together with some early results.

### 2. HRPD DETECTOR

#### 2.1 Geometry and Construction

The main features of the HRPD were given at the ICANS IV meeting<sup>[3]</sup> and a more recent summary of the instrument parameters is given in reference [4] from which the schematic representation shown in Figure 1 is reproduced.

The detector has an annular ring geometry and is used in backscattering, the incident neutron beam passing through a central aperture. The main dimensions are shown in Figure 2. The detector is constructed in identical octants each with 20 rings. Each ring is in the form of 2 layers of 1 mm thick lithium glass scintillator. These layers are coded as separate detectors, the total number of rings thus being 40. The cross-section shown in Figure 2 illustrates the method of gluing the rings together, resulting in a conical shaped nest of rings (see Figure 3). The fibre optic bundles, after coding, are potted in resin and machined off as shown in Figure 4. This face forms a vacuum seal so that the photomultiplier tubes (PM's) can be operated at atmospheric pressure, thus avoiding any vacuum breakdown problems. The detector is mounted in a vacuum vessel which is separated from the sample chamber by an aluminium window (0.5 mm thick). The vessels are pumped down simultaneously to avoid a pressure differential across the window. This arrangement allows a low

pressure to be achieved in the sample volume without the outgassing load produced by the detector itself. The window also completes the lighttight enclosure for the detector - there is no separate lighttight window over the scintillator array itself.

The electronic system is the same as that described in reference [2].

## 2.2 TOF Spectra from SNS

Two octants of the detector are installed in HRPD at the time of writing. The first results were obtained in December 1984 when the SNS operated for a brief run at very low intensity. Two samples were simultaneously in the beam viz: Ni powder at the 1m sample position and a pyrolytic graphite single crystal at the 2m position. A presentation of these results is given in Figure 5 which shows sections (about 1/40 of the total) of the time-of-flight spectra from each of the 20 rings on an octant with the 2 layers of scintillator in each ring summed. These results show that the backgrounds seen by the detector are acceptably low and that there is negligible crosstalk between rings, i.e. a T-O-F peak in one ring does not lead to significant counts in another ring at the same time.

The detection efficiency has not yet been carefully measured. The stopping power,  $\eta$ , of a 2 mm thickness of GS20 scintillator is given by.

$$\eta = (1 - e^{-1.66\lambda})$$

where  $\lambda$  is the neutron wavelength in Å. Approximately 10% of the stopped neutrons do not produce counts due to optical and discrimination losses. Using these values, a comparison between the theoretical and measured intensities of several reflections from nickel powder was made in reference [5] with fair agreement.

The intrinsic background count rate from the detector, i.e. the count rate with no neutron sources present, is about 0.4 counts per minute per  $\text{cm}^2$  of scintillator. There has been no evidence of any problems due to  $\gamma$ -ray background.

### 3. LOQ DETECTOR

#### 3.1 Geometry and Construction

The general arrangement of LOQ is shown schematically in Figure 6 and a description of the instrument as it will be for early SNS operations is given in reference [4]. The main detector consists of concentric rings of scintillator elements of annular width  $\Delta R$  at radius  $R$  such that  $\Delta R/R$  is constant at 0.0358. The azimuthal resolution varies from  $20^\circ$  in the centre of the detector to  $2^\circ$  at the outside as shown in Figure 7 which is a diagram of a 1/9 module. The number of elements per module is 560 coded to 16 PM's, i.e. 5040 elements and 144 PM's in the whole of the main detector. A central aperture allows the unscattered incident beam to pass through to a beam stop.

The detector modules are constructed by first cementing a row of 0.5m diameter fibres side by side in a jig to make up a single layer bundle equal in width to a particular scintillator tile. The scintillator tile itself is then cemented, by its edge, to the fibre bundle via a 5 mm long, 0.5 mm thick, glass light guide. The purpose of the latter is to ensure that the intensity of the scintillator light pulses entering the fibres is reasonably uniform from fibre to fibre. If this is not done, a neutron capture in the scintillator close to a fibre causes a large light pulse input to that fibre but only a very small one into other fibres, since light can only arrive at these within the acceptance angle by transmission through the scintillator tile and reflection back from an edge.

It is believed that in these circumstances the intense light can be reflected from the PM end of the fibre bundle back along other fibres and then back into other PM's giving rise to crosstalk between elements. Two other precautions are taken to minimise this effect. Firstly the edges of the scintillator tiles are coated with a white diffuse reflector to avoid specular reflection of returned photons back into the fibres. Secondly, at the PM end, the fibre bundles are cut at an angle so that light emerging into the PM is not reflected normally (from bright surfaces inside the PM) back up the fibres.

Each arc of elements, with its fibre optic bundles attached, was glued to a backing made as a  $B_4C$ /resin casting to provide some absorber for neutrons not stopped in the scintillator. For the first module, each arc was tested separately on a laboratory neutron source in a special test rig. Good results for uniformity of response were achieved for all the arcs. Figure 8 shows the result of exposing the arc of elements beginning with number 281 to an approximately uniform neutron flux from a Pu/Be source.

The scintillator used is GS20, 0.5 mm thick, giving a stopping power for neutrons of wavelength  $2\text{\AA}$  (the minimum for LOQ) of 57%.

As for the HRPD detector, the fibre optic bundles are taken, after coding, through a vacuum seal so that the PM's can operate at atmospheric pressure. Since the whole secondary flight path and detector are in a large vacuum vessel, the PM's are housed in a sealed box connected to the outside of the vessel by long flexible bellows, which carries the high voltage supplies and signal leads. This arrangement circumvents any problems associated with operating high voltage equipment in vacuum. Since there are signal cable runs of about 10m between the detector modules and the first signal processing electronics situated outside the detector vacuum tank, a preamplifier is built into each PM base. A low airflow is driven through the flexible bellows to remove the small amount of heat (about 70W) generated by the PM dynode resistor chains and the pre-amplifiers.

### 3.2 Results of Laboratory Tests

Figure 9 shows the result of exposing the whole detector module to the laboratory source. The counts seen vary as the area of the elements, as expected.

An overnight background count in the laboratory with the detector module shielded with a 15 cm thickness of borated resin blocks and no neutron sources present showed an intrinsic background between 0.5 and 0.8 counts per minute per  $\text{cm}^2$  of scintillator.

Exposure to a  $^{60}\text{Co}$  source showed a  $\gamma$ -ray counting efficiency of  $1.3 \times 10^{-3}$ .

#### 4. CONCLUSIONS

First results from the HRPD detector system on the SNS have been encouraging. This instrument operates on the end of a 95m long guide tube and is thus in a low  $\gamma$  ray field, an environment particularly suitable for this type of detector system. The intrinsic background counts produced by the detector and the degree of crosstalk between channels have, so far, been adequately low.

First results from the LOQ module on test with a laboratory source have also been good. It is expected that this detector will also operate in a low  $\gamma$ -ray field since the LOQ beam line does not have a line of sight to the SNS cold moderator but incorporates a supermirror bender.

At the time of writing further commissioning tests will be made on both systems, especially at higher neutron beam intensities, before constructing the remainder of the detector modules.

#### 6. ACKNOWLEDGEMENTS

The authors would like to thank Mr B Holland for his highly skilled assistance with the construction of the LOQ module and Mr A Gibbs for his careful work on the HRPD construction.

#### 7. REFERENCES

1. KENS Report II, March 1981, pp 642-654
2. Position-Sensitive Detection of Thermal Neutrons, P Convert and J B Forsyth (Eds), Academic Press (London), p166 (1983)
3. KENS Report II, March 1981 pp 549-555
4. Neutron Scattering Instruments at the SNS - A Guide for Potential Users, February 1985
5. First Neutron Results from SNS, A J Leadbetter et al, RAL-85-030

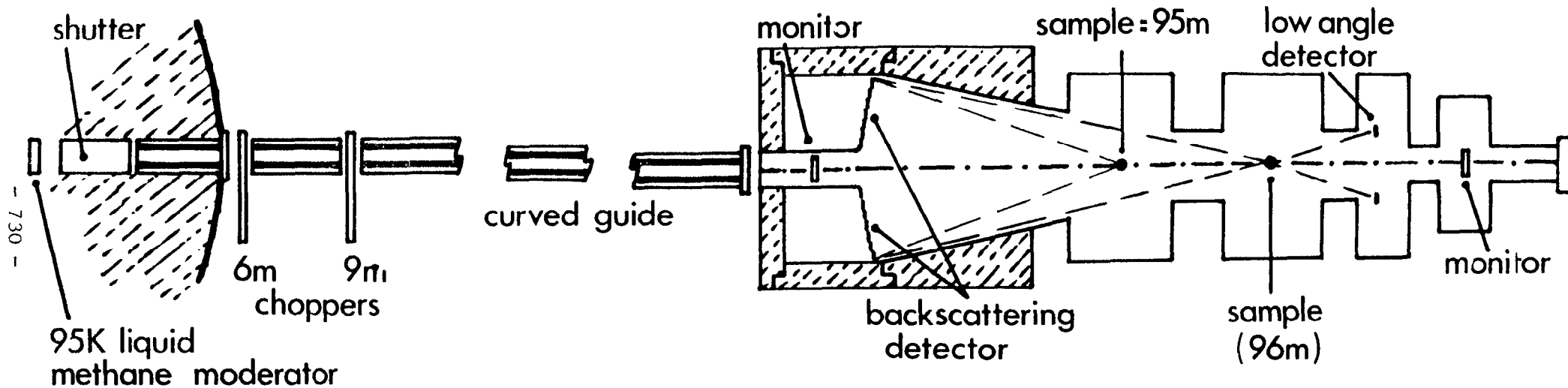
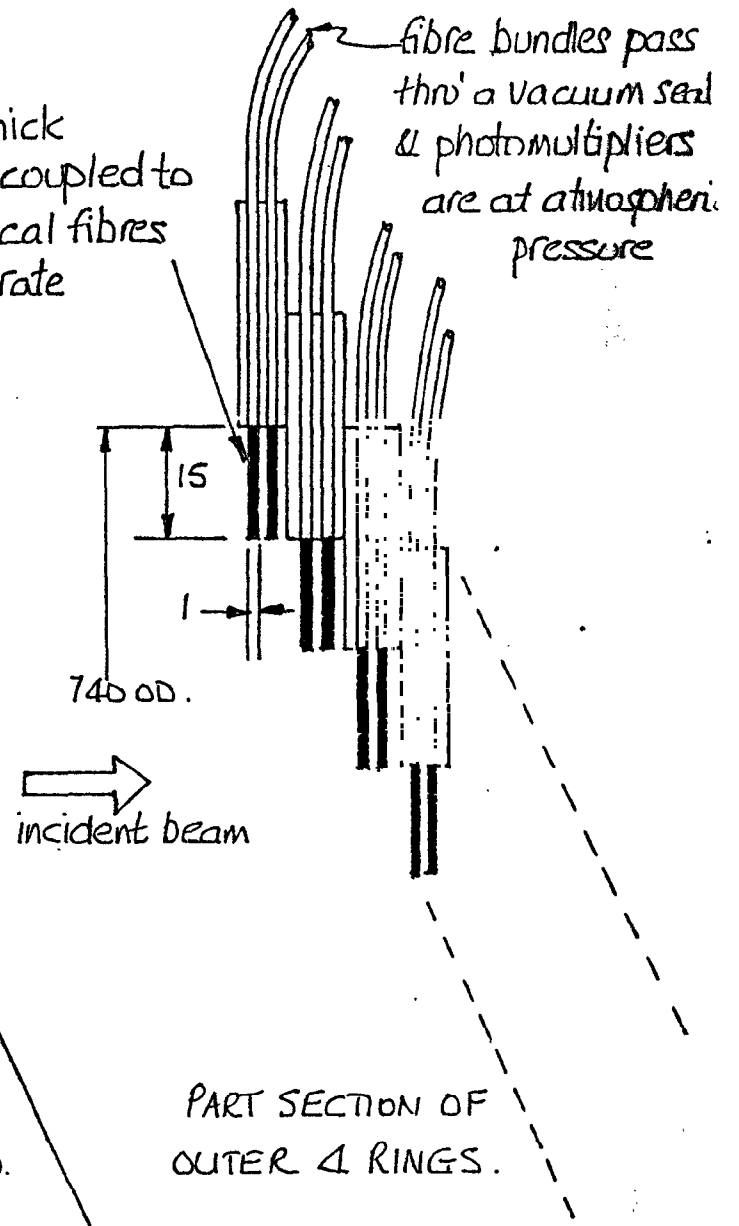
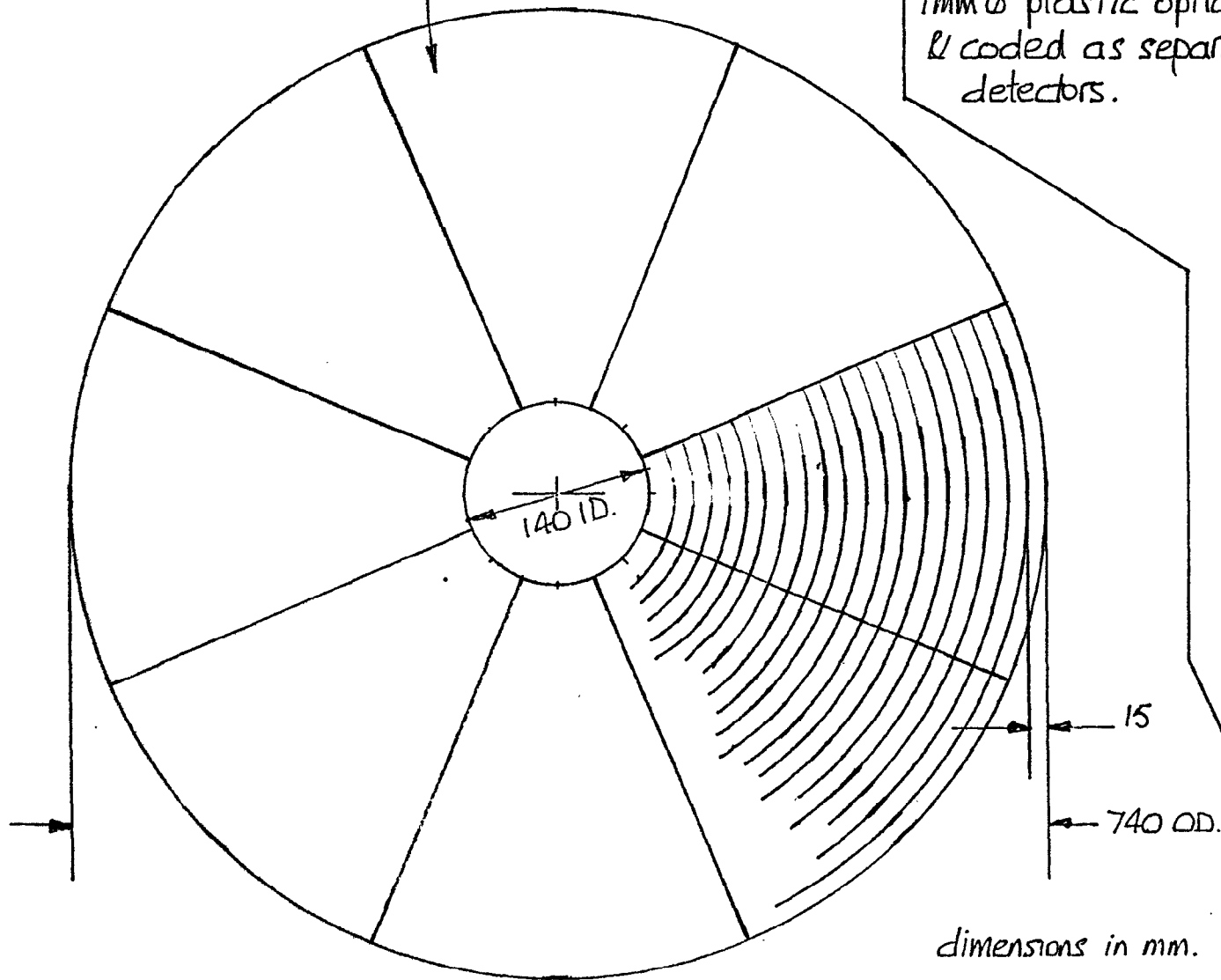


FIG.1. Schematic layout of HRPD.

Whole detector assembled as  
8 separate segments

2 layers of 1mm thick  
glass scintillator coupled to  
1mm  $\phi$  plastic optical fibres  
& coded as separate  
detectors.

fibre bundles pass  
thru a vacuum seal  
& photomultipliers  
are at atmospheric  
pressure



PART SECTION OF  
OUTER 4 RINGS.

dimensions in mm.

FIG.2 Geometry of HRPD detector



FIG.3 HRPD encoder showing scintillator end before cementing on scintillator tiles.





FIG.4 HRPD encoder showing PM end of fibre bundles  
before installing P.M. tubes.

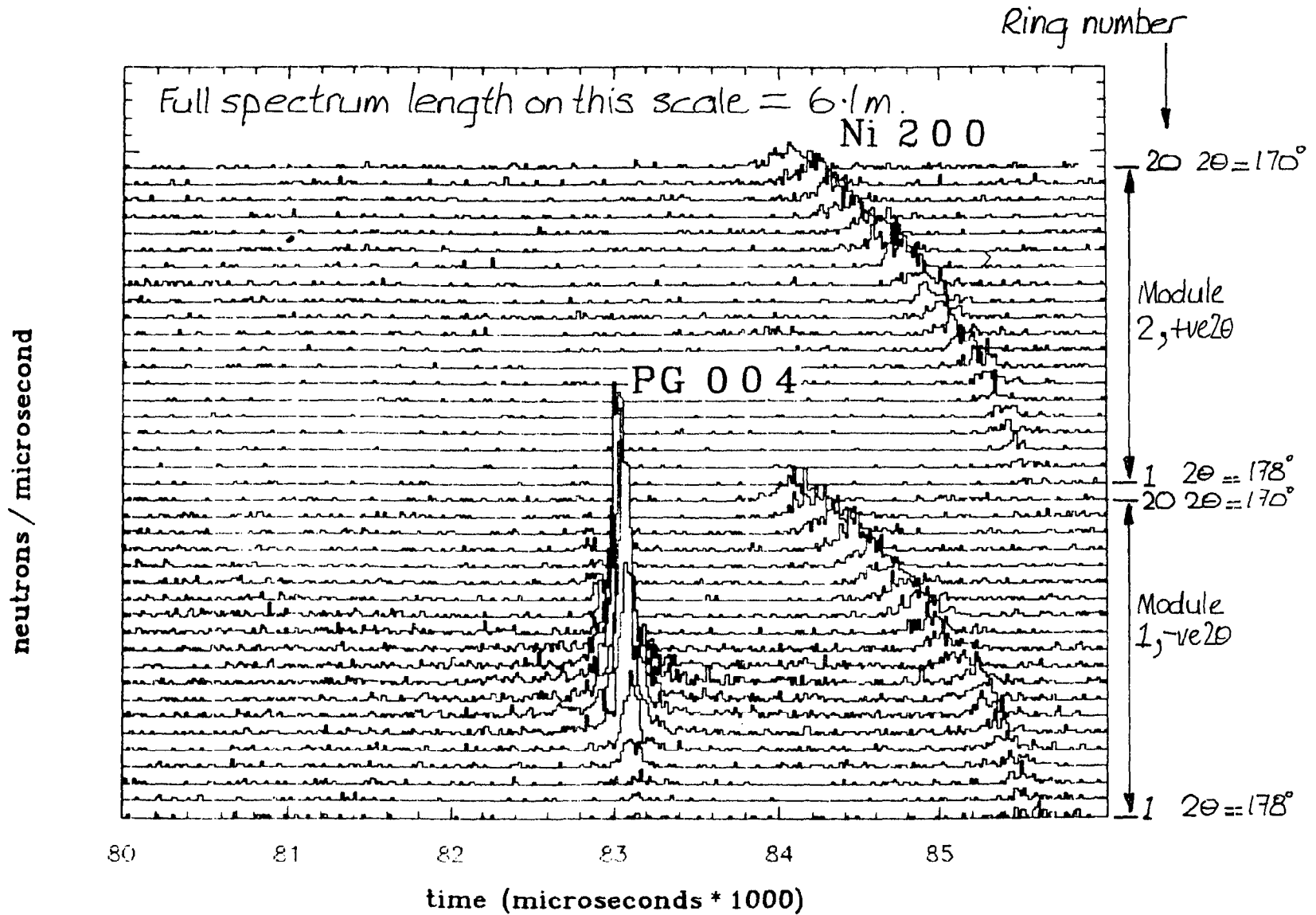


FIG.5 Time of flight spectra from HRPD with nickel powder and pyrolytic graphite single crystal samples.

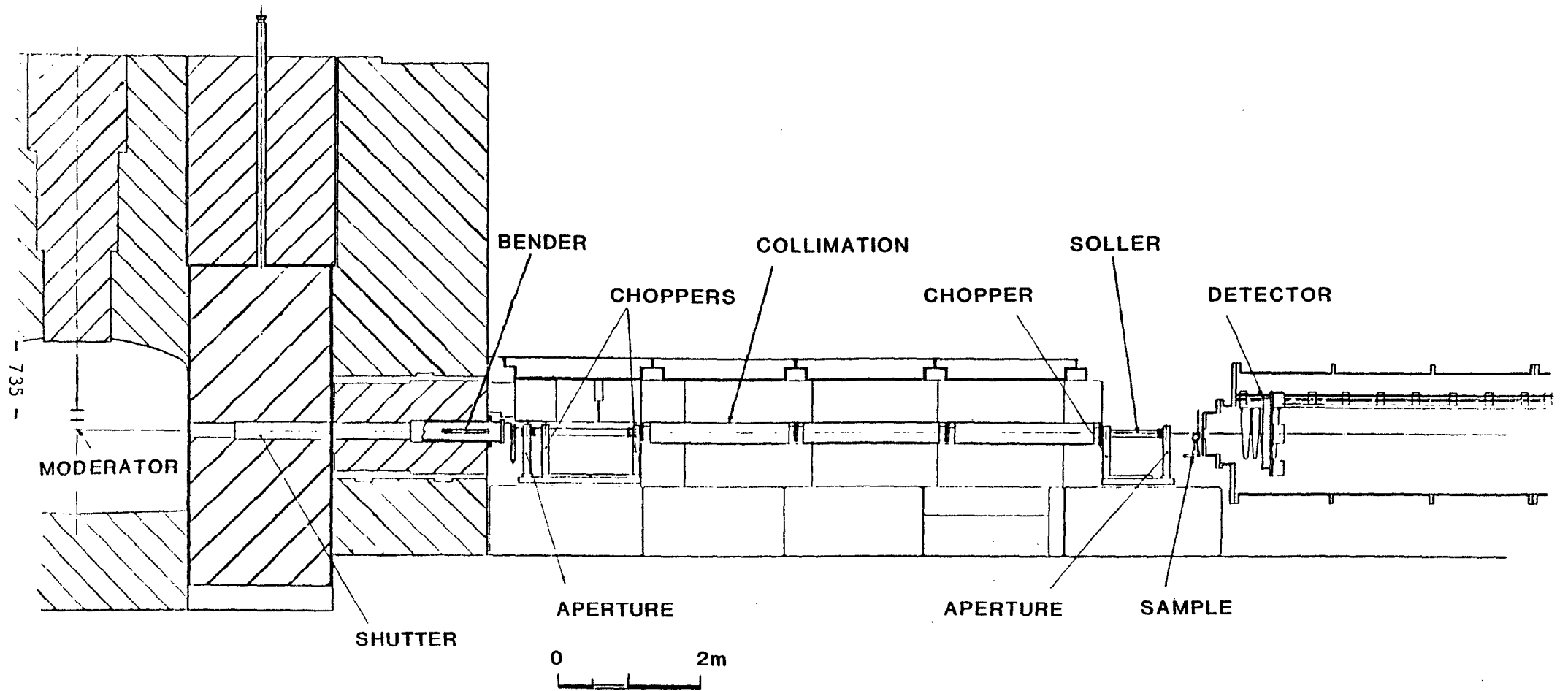


FIG. 6 *Schematic layout of LOQ*

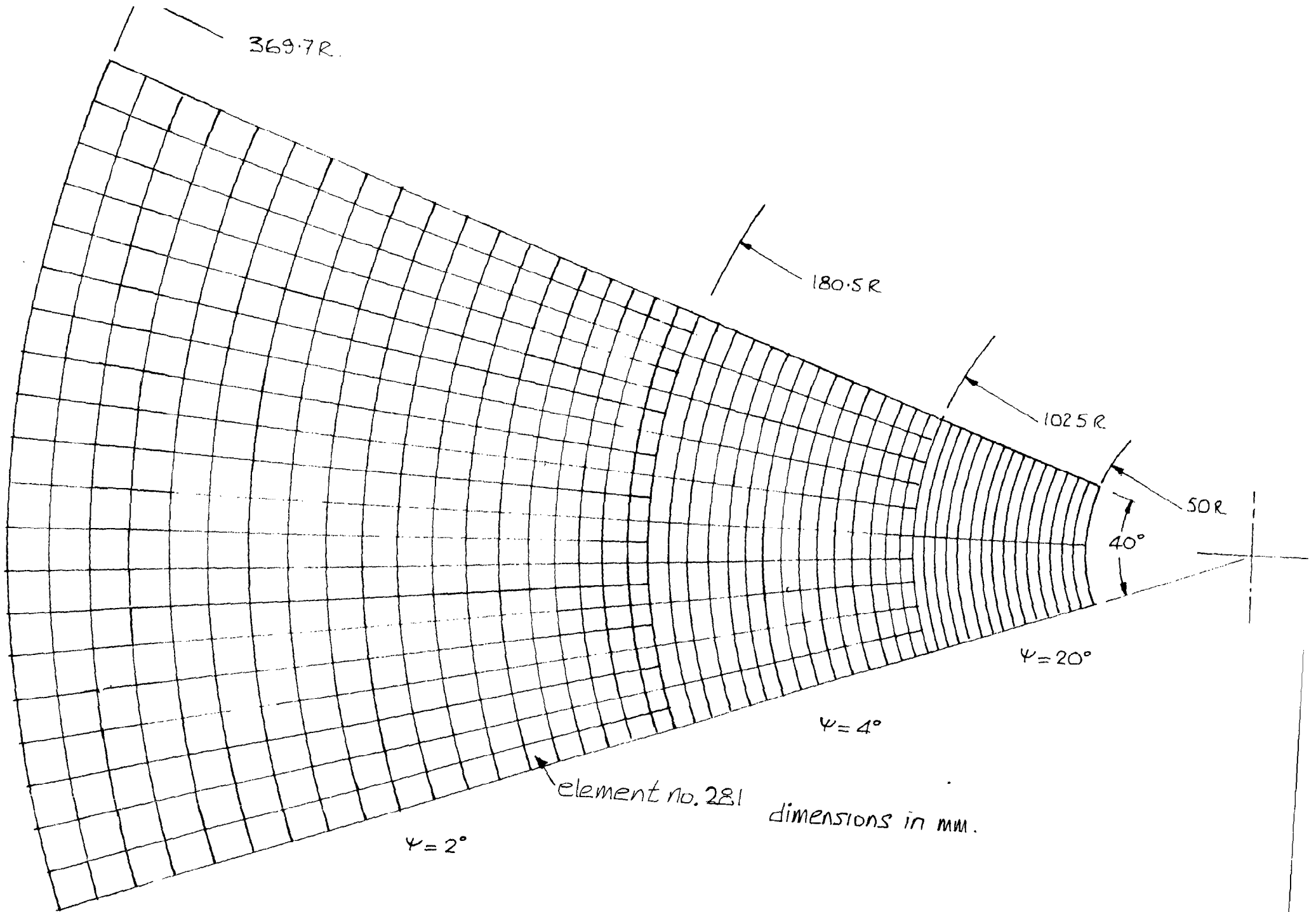


FIG. 7 Geometry of a 1/3 module of the LOQ

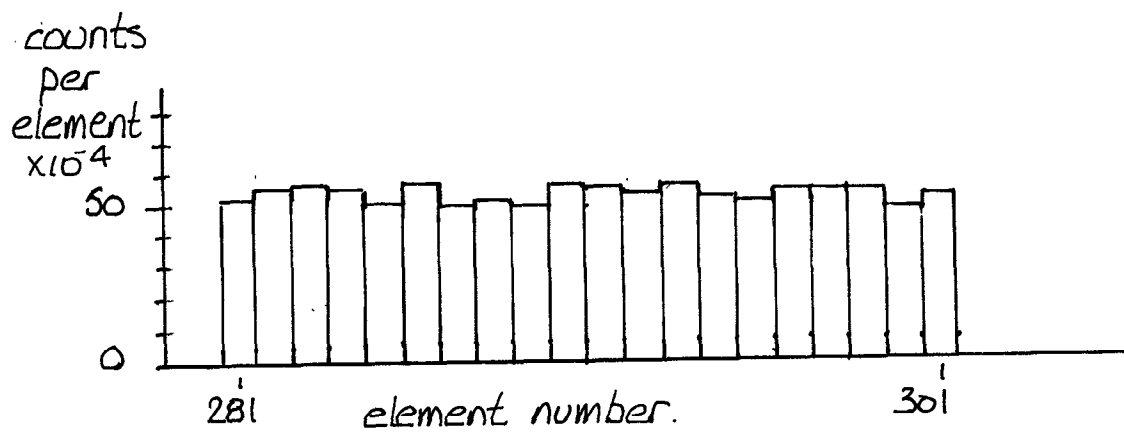


FIG. 8 Response of an arc of LOQ detector elements to a laboratory neutron source.

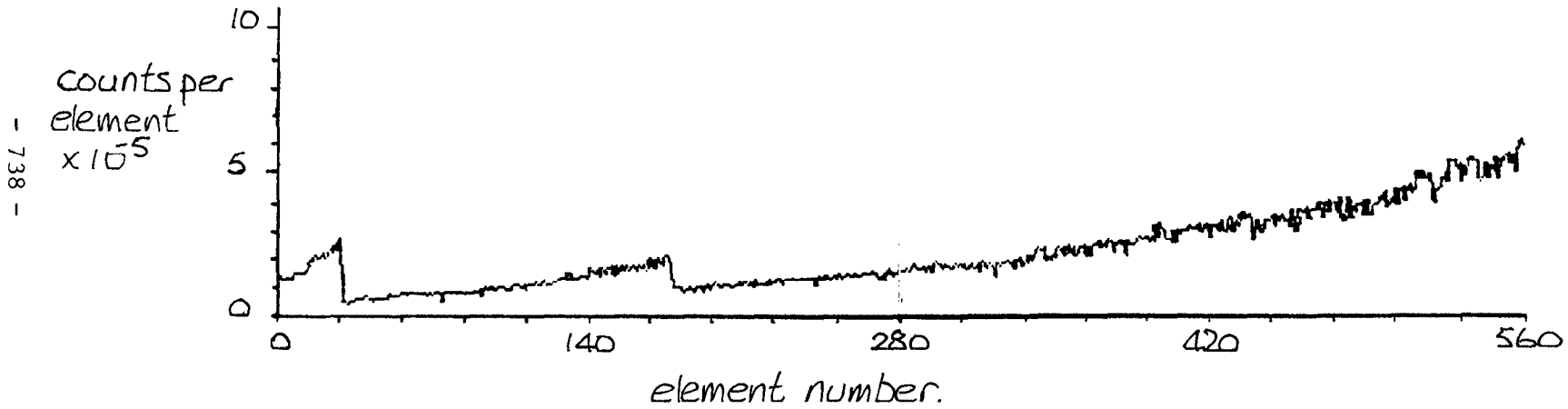


FIG. 9

Response of a  $\frac{1}{9}$  module of the LOQ main detector to a laboratory neutron source.